Mon. Not. R. Astron. Soc. **379,** 357–369 (2007) doi:10.1111/j.1365-2966.2007.11961.x

# Multiwavelength study of X-ray selected star-forming galaxies within the *Chandra Deep Field*-South

Daniel Rosa-González,[1⋆] Denis Burgarella,[2] Kirpal Nandra,[3] Daniel Kunth,[4] Elena Terlevich[1]† and Roberto Terlevich[1]†

[1]*INAOE, Luis Enrique Erro 1, Tonantzintla, Puebla 72840, México*
[2]*Observatoire Astronomique Marseille Provence, Laboratoire d'Astrophysique de Marseille, 13376 Marseille Cedex 12, France*
[3]*Astrophysics Group, Imperial College London, Blackett Laboratory, Prince Consort Road, London SW7 2AW*
[4]*Institut d'Astrophysique, Paris, 98 bis Boulevard Arago, F-75014 Paris, France*

Accepted 2007 May 7. Received 2007 April 18; in original form 2006 November 9

**ABSTRACT**

We have combined multiwavelength observations of a selected sample of star-forming galaxies with galaxy evolution models in order to compare the results obtained for different star formation rate (SFR) tracers and to study the effect that the evolution of the star-forming regions has on them. We also aimed at obtaining a better understanding of the corrections due to extinction and nuclear activity on the derivation of the SFR. We selected the sample from *Chandra* data for the well studied region *Chandra Deep Field*-South (CDFS) and chose the objects that also have ultraviolet (UV) and infrared (IR) data from *Galaxy Evolution Explorer* (*GALEX*) and Great Observatories Origins Deep Survey (GOODS) *Spitzer*, respectively.

Our main finding is that there is good agreement between the extinction corrected SFR(UV) and the SFR(X), and we confirm the use of X-ray luminosities as a trustful tracer of recent star formation activity. Nevertheless, at SFR(UV) larger than about $5\,M_{\odot}\,yr^{-1}$ there are several galaxies with an excess of SFR(X) suggesting the presence of an obscured active galactic nucleus (AGN) not detected in the optical spectra. We conclude that the IR luminosity is driven by recent star formation even in those galaxies where the SFR(X) is an order of magnitude higher than the SFR(UV) and therefore may harbour an AGN. One object shows SFR(X) much lower than expected based on the SFR(UV); this SFR(X) 'deficit' may be due to an early transient phase before most of the massive X-ray binaries were formed. An X-ray deficit could be used to select extremely young bursts in an early phase just after the explosion of the first supernovae associated with massive stars and before the onset of massive X-ray binaries.

**Key words:** galaxies: fundamental parameters – ultraviolet: galaxies – X-rays: galaxies.

## 1 INTRODUCTION

The ultraviolet (UV) emission in galaxies traces the presence of massive stars related to a recent episode of star formation. For this reason, the UV luminosity is widely used as a tracer of the star formation activity not only in nearby galaxies but also in the early Universe (e.g. Lilly et al. 1995; Madau et al. 1996). However, it is important to bear in mind that the corrections applied to the observed UV fluxes (e.g. due to extinction and evolutionary uncertainties) are neither unique nor straightforward implying that multiwavelength studies are necessary to improve the correction factors (e.g. Buat et al. 2005; Schmitt et al. 2006).

⋆E-mail: danrosa@inaoep.mx
†Research Affiliate IoA, Cambridge, UK.

The X-ray emission in normal galaxies – without an active galactic nucleus (AGN) component – is produced by high-mass X-ray binaries (HMXB), low-mass X-ray binaries (LMXB), young supernova remnants (SNRs) and cooling hot gas (e.g. Fabbiano 1989). The relation between the observed X-ray luminosities and the current star formation rate (SFR) is driven by the presence of HMXB where the primary star is a collapsed object with mass higher than $2.5\,M_{\odot}$ and the secondary star is a massive star classified as O, B or Wolf Rayet (Van Bever & Vanbeveren 2000; Cerviño, Mas-Hesse & Kunth 2002). Because of the strong correlation found between the X-ray luminosity and other tracers of recent star formation activity such as the far-infrared (FIR) luminosity (David, Jones & Forman 1992), the radio emission (Ranalli, Comastri & Setti 2003) and the number of HMXB (Grimm, Gilfanov & Sunyaev 2003), the X-ray luminosity has been used to calculate the SFR even at high redshift (Nandra et al. 2002; Laird et al. 2005). However, at large

distances, it is difficult to separate the different contributors to the X-ray luminosity, hence the estimated SFR could be jeopardized by the presence of obscured AGN unnoticed in the optical spectral range and also by LMXB which are not related to the recent star formation event.

In addition, in very young systems we expect to observe a deviation of the SFR given by the X-ray luminosities [SFR(X)] with respect to the SFR given by the UV [SFR(UV)] due to the different time-scales for the emission from massive stars – responsible for the UV (e.g. Mas-Hesse & Kunth 1991) – and the formation of the first HMXB which dominate the X-ray luminosities. These different time-scales would produce a time lag between the UV and X-ray emission – depending on the upper mass of the initial mass function (IMF) of the ionizing cluster – of at least a few million years. Notice that stars with masses higher than about 8 $M_\odot$ end their lives as supernovae after about 40 Myr when they might form a binary system. Therefore, the existence of a time lag between the formation of the massive stellar cluster and the formation of the first compact object that could end as a binary system opens an opportunity to use the lack of X-rays to search for young objects of between 4 and up to ∼40 Myr. The lag between the formation of the first massive stars and the formation of compact objects has been already successfully used to find young objects using deep radio observations in which – as in the case of X-rays – the radio emission from SNRs is produced after some million years of the formation of the stellar cluster (Rosa-González et al. 2007).

Multiwavelength observations of the *Chandra Deep Field*-South (CDFS) – one of the best studied patches of the sky – have contributed to our understanding of fundamental processes in galaxy evolution (e.g. Giacconi et al. 2001; Tozzi et al. 2001; Gabasch et al. 2004; Adami et al. 2005; Ferreras et al. 2005). In this paper we focus on the relation between the observed UV and X-rays based on archival data provided by the Great Observatories Origins Deep Survey (GOODS) for the CDFS, to study in detail the relation between the SFR(UV) and the SFR(X). We also include data obtained from the *Spitzer* archives for estimating the star formation based on infrared (IR) luminosities [SFR(IR)] and to put stringent limits on the extinction corrections applied to the UV fluxes.

This paper is organized in the following way: in Section 2 we describe the galaxy sample; the method adopted to obtain UV fluxes is presented in Section 3 and in Section 4 we obtain the SFR from UV and X-ray luminosities. The contamination by AGN and the existence of fainter than expected X-ray galaxies are discussed in Section 5. Section 6 describes the FIR data of our subsample of galaxies detected with *Spitzer* and the derived SFR(IR). Conclusions are presented in Section 7.

Throughout this work a standard, flat Λ cold dark matter (ΛCDM) cosmology with $\Omega_\Lambda = 0.7$ and $H_0 = 70\,\mathrm{km\,s^{-1}\,Mpc^{-1}}$ is assumed.

## 2 THE SAMPLE

The CDFS, centred in coordinates $\alpha_{2000} = 03^{\mathrm{h}}32^{\mathrm{m}}25^{\mathrm{s}}$ and $\delta_{2000} = -27^\circ48'50''$, was observed during 942 ks using the Advanced CCD Imaging Spectrometer on board the *Chandra* X-Ray Observatory. The CDFS data also include optical identifications based on *R*-band imaging of the field (Giacconi et al. 2002; Rosati et al. 2002; Alexander et al. 2003). We cross-correlated the *Chandra* observations of the CDFS with UV data from the *Galaxy Evolution Explorer* (*GALEX*).

*GALEX* is a NASA Small Explorer Mission launched on the 2003 April 28 developed in cooperation with the Centre National d'Etudes Spatiales of France and the South Korean Ministry of Science and Technology. It was designed to perform several surveys in two UV bands: FUV (far-UV) centred at 1530 Å and NUV (near-UV) at 2310 Å. The detailed characteristics of *GALEX* are given in Morrissey et al. (2005). In brief, with a very wide 1.°25 field of view and an angular resolution of ∼5 arcsec [full width at half-maximum (FWHM)], *GALEX* is performing the first UV All-Sky Imaging Survey (AIS) down to $m_{AB} = 20.5$. The *GALEX* data at 2312 Å (NUV) and 1522 Å (FUV) used in this work were obtained directly from the Multimission Archive at the Space Telescope Science Institute (MAST)[1] and they are part of the *GALEX* Deep Imaging Survey project which reaches a magnitude limit of $m_{AB} = 25$.

Alexander et al. (2003) listed 326 CDFS sources of which 293 were detected in the soft band (0.5–2 keV), 198 in the hard band (2–10 keV) and 174 in both. We searched for the *GALEX* counterpart in a circle of 5-arcsec radius including the position errors both in *GALEX* and in *Chandra*. We were left with a preliminary subsample of 59 objects that includes only those detected in the two *GALEX* bands. Some objects that are just upper limits in one or both of *Chandra* bands were still retained in the analysis that follows. Notice that these weak sources were extracted from the main catalogue by Alexander et al. (2003) where an X-ray source is defined as an object that is detected with a false-positive probability higher than $10^{-7}$, at least in one of the seven standard bands defined in their paper. This first selection would have excluded most of the obscured AGNs contained in early-type galaxies, and also star-forming galaxies with redshift larger than about 1. The following step was to use the broad photometric classification given by the Classifying Objects by Medium-Band Observations (COMBO-17) team[2] to select only objects classified as galaxies excluding quasi-stellar object (QSO) or Seyfert 1. The COMBO-17 classification is based on both the size of the image and the colours of the object. Objects with clearly extended morphology are classified as galaxies while compact objects which present a power-law continuum are classified as QSO (Wolf et al. 2004). After inspection of the provided images (optical and UV) we removed those objects for which the *GALEX* source was not univocally associated to an optical counterpart. In Table 1 we present the final sample of 29 galaxies including CDFS 132, for which both X-ray fluxes are considered upper limits.

The separations between the *Chandra* and the corresponding *GALEX* source are smaller than 3 arcsec except for CDFS 213 and CDFS 325. For these galaxies we check the positions given by Giacconi et al. (2002) and found that they lie closer to the optical counterpart. Different position determinations are expected when different extraction methods are used on diffuse weak sources. The fluxes provided by these authors for these sources are similar in both soft and hard band; for the soft X-rays flux of CDFS 213, Alexander et al. considered the value as an upper limit while Giacconi et al. give the soft X-ray flux as a detection.

As we mentioned above, some of the *Chandra* detections are only upper limits but we left them in the sample as they have been detected by *GALEX* in the two UV bands.

Table 1 lists UV and X-ray fluxes of the selected objects. It also includes the corresponding *R* band and the photometric redshift based on COMBO-17 observations when spectroscopic data were not available. The COMBO-17 observations of the CDFS include five different broad-band filters (*U*, *B*, *V*, *R* and *I*) and 12 narrow

[1] http://archive.stsci.edu

[2] COMBO-17 (a spectrophotometric 17-filter survey) is a photometric survey performed with the MPG/ESO (Max Planck Gesellschaft/European Southern Observatory) 2.2-m telescope at La Silla, Chile (Wolf et al. 2004).

**Table 1.** X-ray and UV characteristics of the selected objects. The columns are object name, separation between *Chandra* and *GALEX* positions (*Chandra* positions are from Alexander et al. 2003; in parenthesis, distances using positions by Giacconi et al. 2002), flux and luminosity in the soft and hard X-ray bands, [a]NUV, FUV, *R* band and photometric redshift (spectroscopic redshift in bold if available). Units of the X-ray fluxes are $10^{-15}$ erg s$^{-1}$ cm$^{-2}$.

| Name | Separation (arcsec) | $F_{0.2-2\,\mathrm{keV}}$ | $F_{2-10\,\mathrm{keV}}$ | Log $L_{0.2-2\,\mathrm{keV}}$ (erg s$^{-1}$) | Log $L_{2-10\,\mathrm{keV}}$ (erg s$^{-1}$) | NUV (μJy) | FUV (μJy) | $R$ (mag) | $z$ |
|---|---|---|---|---|---|---|---|---|---|
| CDFS 017 | 0.47 | 1.08 | 2.59 | 42.60 | 42.98 | 0.99 | 0.30 | 21.42 | $0.724 \pm 0.045$ |
| CDFS 065 | 1.19 | <0.09 | 1.14 | <40.54 | 41.64 | 1.32 | 0.90 | 19.22 | **0.310** |
| CDFS 073 | 0.80 | 0.10 | <0.76 | 40.98 | <41.86 | 1.07 | 0.66 | 19.36 | $0.440 \pm 0.013$ |
| CDFS 078 | 2.93 | 1.88 | 3.94 | 41.29 | 41.61 | 8.97 | 4.33 | 19.58 | $0.180 \pm 0.009$ |
| CDFS 088 | 0.82 | 2.48 | 18.73 | 42.74 | 43.62 | 3.85 | 0.74 | 20.16 | **0.605** |
| CDFS 129 | 0.14 | 0.22 | <0.94 | 40.61 | <41.24 | 1.61 | 1.37 | 19.18 | **0.229** |
| CDFS 132 | 0.93 | <0.06 | <0.32 | <40.06 | <40.78 | 6.19 | 4.24 | 20.37 | **0.232** |
| CDFS 149 | 0.50 | 0.23 | 0.75 | 40.06 | 40.57 | 4.67 | 2.97 | 20.12 | **0.131** |
| CDFS 152 | 0.56 | 0.06 | <0.26 | 40.13 | <40.76 | 10.28 | 7.66 | 19.89 | **0.248** |
| CDFS 158 | 1.04 | 0.09 | <0.33 | 40.71 | <41.28 | 3.32 | 0.93 | 20.71 | **0.363** |
| CDFS 167 | 0.84 | 0.09 | <0.58 | 41.24 | <42.05 | 1.73 | 0.52 | 20.52 | **0.577** |
| CDFS 185 | 1.02 | 0.06 | <0.42 | 40.93 | <41.77 | 2.80 | 1.37 | 22.20 | **0.511** |
| CDFS 189 | 0.88 | 0.81 | <0.34 | 40.07 | <39.70 | 62.46 | 41.54 | 16.55 | $0.075 \pm 0.01$ |
| CDFS 192 | 0.90 | 0.57 | 0.71 | 40.05 | 40.14 | 35.35 | 23.69 | 17.06 | $0.086 \pm 0.012$ |
| CDFS 196 | 0.68 | 0.07 | <0.37 | 41.31 | <42.03 | 1.40 | 0.25 | 21.46 | **0.667** |
| CDFS 207 | 0.81 | 0.18 | 0.93 | 39.83 | 40.54 | 4.75 | 3.16 | 17.08 | $0.115 \pm 0.005$ |
| CDFS 213 | 4.90(3.02) | 0.12 | 1.50 | 39.00 | 40.10 | 30.49 | 22.34 | 16.19 | $0.058 \pm 0.003$ |
| CDFS 228 | 0.52 | 0.15 | <1.21 | 39.88 | <40.79 | 2.50 | 0.61 | 18.23 | $0.132 \pm 0.01$ |
| CDFS 236 | 0.47 | 0.08 | <0.31 | 40.92 | <41.51 | 5.57 | 2.70 | 20.97 | **0.456** |
| CDFS 238 | 0.76 | 0.06 | <0.29 | 40.10 | <40.78 | 1.55 | 1.02 | 20.10 | **0.241** |
| CDFS 240 | 0.55 | 1.98 | 37.83 | 41.86 | 43.14 | 2.91 | 0.65 | 18.86 | $0.304 \pm 0.003$ |
| CDFS 265 | 1.35 | 0.14 | <0.60 | 41.19 | <41.82 | 6.04 | 1.51 | 19.47 | $0.467 \pm 0.008$ |
| CDFS 267 | 0.39 | 0.11 | 0.21 | 39.30 | 39.58 | 9.54 | 7.86 | 20.27 | $0.083 \pm 0.005$ |
| CDFS 270 | 0.96 | 0.89 | <0.85 | 40.52 | <40.50 | 8.25 | 2.40 | 16.07 | $0.115 \pm 0.005$ |
| CDFS 291 | 0.94 | 0.22 | <0.64 | 39.83 | <40.29 | 22.84 | 16.62 | 17.11 | **0.105** |
| CDFS 292 | 0.45 | 0.22 | <0.72 | 41.11 | <41.63 | 20.97 | 13.28 | 19.87 | **0.366** |
| CDFS 294 | 0.25 | 0.23 | <0.81 | 39.95 | <40.50 | 17.21 | 15.24 | 18.03 | $0.117 \pm 0.006$ |
| CDFS 304 | 0.92 | 1.00 | 9.23 | 41.93 | 42.90 | 1.41 | 0.88 | 20.35 | **0.424** |
| CDFS 325 | 3.57(1.4) | 1.45 | 5.62 | 41.87 | 42.46 | 5.27 | 2.81 | 19.88 | **0.347** |

[a]CDFS sources have been detected in at least one of the seven bands defined in Alexander et al. (2003) (see text).

filters necessary to constrain the photometric redshifts with an accuracy of about 5 per cent at $z \lesssim 1$ (Wolf et al. 2004). The optical broad-band data are presented in Table 2.

The spectroscopic redshift ($z_{\mathrm{sp}}$) comes from Szokoly et al. (2004) except for CDFS 132 and CDFS 185 for which $z_{\mathrm{sp}}$ comes from the recent work by Ravikumar et al. (2007).

## 3 EXTINCTION-CORRECTED UV FLUXES FROM TEMPLATE FITTING

To obtain the intrinsic UV flux at rest frame 2000 Å from the optical spectra and UV observed values, we adopted a template fitting approach (Bolzonella, Miralles & Pelló 2000; Babbedge et al. 2004). We used five different galaxy templates calculated with the GRASIL code (Silva et al. 1998) that are accessible from a library of galaxy models.[3] The extinction-free templates represent spirals (Sa, Sb and Sc) and the starburst galaxies M82 and Arp 220. Notice that, for spirals, the obtained galaxy type represents an average of the observed spectral energy distribution (SED), but due to the large dispersion present in most of the observables (e.g. absolute magnitudes, colours) and in derived physical properties (like star formation history) we cannot unequivocally assign a morphological type to a single spectrum. Therefore, the galaxy templates just correspond to an average of the intrinsic stellar emitted light without extinction; we do not attempt to fit as well a galaxy type.

[3] http://web.oapd.inaf.it/granato/grasil/modlib/modlib.html

From the comparison of models and observations we obtained the best match using a $\chi^2$ minimization. The observed data included the five optical bands (Table 2) provided by Wolf et al. (2004) plus the two UV *GALEX* bands. For each object the original GRASIL template was shifted according to the $z_{\mathrm{sp}}$ or the COMBO-17 photometric redshift. The observed flux $F_{\mathrm{o}}(\lambda)$ and the flux given by the template, $F_{\mathrm{t}}(\lambda)$ can be expressed as a function of the extinction as (e.g. Osterbrock 1989)

$$F_{\mathrm{o}}(\lambda) = F_{\mathrm{t}}(\lambda) \times 10^{-0.4 A_V k(\lambda)/R}, \quad (1)$$

where the values $k(\lambda)$ and $R$ are tabulated for different extinction curves. It is known that the appropriate extinction curve for local galaxies depends on the type of galaxy and on parameters, such as metallicity, that presumably determine the characteristics of the dust. These parameters are not known for the selected sample, so we included the extinction law as one of the unknowns in the fitting grid. The best fit was found in a three-dimensional grid where we change the galaxy template, the value of the visual extinction ($A_V$) and the extinction curve. For this analysis we adopted three different extinction curves: Milky Way (MW; Seaton 1979; Howarth 1983), Large Magellanic Cloud (LMC; Howarth 1983) and Calzetti law for starburst galaxies (Calzetti; Calzetti, Kinney & Storchi-Bergmann 1994). Unfortunately there is no independent information to further constrain the extinction (e.g. hydrogen emission line ratios) or the morphologies of the galaxies (the optical images provided by COMBO-17 are not good enough for a detailed morphological study).

**Table 2.** Optical magnitudes of the selected objects.

| Name | *I* | *R* | *V* | *B* | *U* |
|---|---|---|---|---|---|
| CDFS 017 | 20.205 | 21.294 | 22.335 | 22.785 | 22.390 |
| CDFS 065 | 18.147 | 19.112 | 20.104 | 21.197 | 21.566 |
| CDFS 073 | 18.255 | 19.258 | 20.525 | 21.511 | 22.229 |
| CDFS 078 | 18.851 | 19.440 | 19.923 | 20.522 | 20.457 |
| CDFS 088 | 19.103 | 20.069 | 21.112 | 21.622 | 21.204 |
| CDFS 129 | 18.308 | 19.064 | 19.822 | 20.799 | 21.122 |
| CDFS 132 | 19.809 | 20.273 | 20.722 | 21.312 | 21.029 |
| CDFS 149 | 19.433 | 20.004 | 20.529 | 21.109 | 21.081 |
| CDFS 152 | 19.376 | 19.784 | 20.221 | 20.774 | 20.355 |
| CDFS 158 | 19.975 | 20.583 | 21.252 | 22.106 | 21.688 |
| CDFS 167 | 19.373 | 20.401 | 21.663 | 22.392 | 22.144 |
| CDFS 185 | 22.012 | 22.130 | 22.811 | 23.069 | 22.199 |
| CDFS 189 | 15.875 | 16.420 | 16.986 | 17.464 | 17.539 |
| CDFS 192 | 16.328 | 16.905 | 17.499 | 18.013 | 18.136 |
| CDFS 196 | 20.823 | 21.363 | 22.175 | 22.516 | 22.043 |
| CDFS 207 | 16.230 | 16.949 | 17.642 | 18.490 | 18.972 |
| CDFS 213 | 15.240 | 16.021 | 16.770 | 17.395 | 17.803 |
| CDFS 228 | 17.371 | 18.073 | 18.758 | 19.548 | 19.883 |
| CDFS 236 | 20.325 | 20.843 | 21.471 | 21.913 | 21.120 |
| CDFS 238 | 19.198 | 20.023 | 20.809 | 21.680 | 21.805 |
| CDFS 240 | 17.919 | 18.710 | 19.466 | 20.550 | 20.878 |
| CDFS 265 | 18.647 | 19.330 | 20.246 | 20.845 | 20.457 |
| CDFS 267 | 19.826 | 20.136 | 20.320 | 20.798 | 20.535 |
| CDFS 270 | 15.190 | 15.934 | 16.637 | 17.505 | 18.027 |
| CDFS 291 | 16.332 | 16.971 | 17.605 | 18.283 | 18.549 |
| CDFS 292 | 19.467 | 19.756 | 20.131 | 20.597 | 19.738 |
| CDFS 294 | 17.264 | 17.895 | 18.482 | 19.143 | 19.301 |
| CDFS 304 | 19.309 | 20.223 | 21.321 | 22.175 | 22.176 |
| CDFS 325 | 18.937 | 19.777 | 20.653 | 21.267 | 21.193 |

The results of the fitting are presented in Table 3 and the individual fitted spectra compared to observed values are plotted in Fig. 1. Once the best fit is obtained we calculate the extinction-corrected UV flux at 2000 Å in the corresponding rest-frame template (Table 3). The provided UV flux corresponds to the rest frame value at 2000 Å and it is directly obtained from the dust-free template taking into account the redshift of the source. A UV excess, that quantifies the deviation of the model from the observed UV values, is calculated by adding the difference between the observed NUV and FUV fluxes and the corresponding values given by the best-fitting model. The obtained quantities, normalized by the sum of the observed UV fluxes and multiplied by 100, are around $\pm 15$ per cent and are indicated as labels to the individual panels in Fig. 1.

The rescaling of the original template to the observed flux in the *I* band gives an estimate of the stellar content of the galaxies (Table 3). However, as the *I* band could be contaminated by the emission of massive stars (red supergiants) which do not contribute significantly to the total mass of the galaxy, the given stellar mass should be treated as an upper limit of the total stellar mass.

## 4 CORRELATION BETWEEN UV AND X-RAY LUMINOSITIES

A strong correlation between the SFR calculated from the UV [SFR(UV)] and from the X-ray luminosities [SFR(X)] in the observed galaxies, if it exists, would suggest, naîvely, that these luminosities are dominated by a young stellar population. Because of different time-scales in the processes involved, however, there is a very early stage when X-rays would not have yet been produced, as has been discussed in the Introduction.

There are several published relations between the UV luminosity and the current SFR that also discuss the difficulty of correcting the observed UV fluxes from extinction (e.g. Madau, Pozzetti & Dickinson 1998; Rosa-González, Terlevich & Terlevich 2002). For solar metallicity and a Salpeter IMF, the SFR(UV) is given by (Kennicutt 1998)

$$\mathrm{SFR(UV)}\,(\mathrm{M_\odot\,yr^{-1}}) = 1.4\times10^{-28} L_{2000}\,(\mathrm{erg\,s^{-1}\,Hz^{-1}}), \quad (2)$$

where $L_{2000}$ is the extinction-corrected luminosity per unit of frequency at the rest-frame wavelength of 2000 Å.

For the X-ray luminosities we adopted the empirical law derived by Ranalli et al. (2003) who combined the existing relations between the SFR and the IR and radio luminosities (Condon 1992; Kennicutt 1998) with the strong correlation between X-ray and IR observed in a sample of local star-forming galaxies,

$$\mathrm{SFR(X)}\,(\mathrm{M_\odot\,yr^{-1}}) = 2.2\times10^{-40} L_{0.2-2\,\mathrm{keV}}. \quad (3)$$

This relation is, within the errors, equal to that by Bauer et al. (2002) based on the correlation between the SFR obtained by radio and the X-ray luminosities of galaxies from the *Chandra Deep Field*-North. Other calibrations of the SFR(X) are based on the HMXB luminosities (e.g. Grimm et al. 2003; Persic et al. 2004). The relation between the integrated luminosity of the HMXBs in the 2–10 keV band strongly correlates with the SFR given by the IR luminosities and shows a very small scatter, smaller in fact than the scatter observed if the total X-ray luminosity is used. However, due to the impossibility of separating the HMXB from the total luminosity we are forced to use Ranalli et al. (2003) empirical relation.

Fig. 2 shows the SFR(X) obtained from equation (3) against SFR(UV). We find that most of the galaxies lie close to the solid line defined as SFR(X) = SFR(UV) even at low values of the SFR(UV) ($\lesssim 5\,\mathrm{M_\odot\,yr^{-1}}$); this contradicts previous claims by Grimm et al. (2003) which are based on the luminosity of HMXB alone. In contrast, we would like to remark that the expression (used by us) given by Ranalli et al. (equation 3) is obtained by direct comparison between radio and IR luminosities and, therefore, it refers to the *total* X-ray luminosity which includes, apart from the contribution due to HMXB and LMXB, the emission from young SNRs and the diffuse hot gas. Notice also that when the X-ray luminosity is low, the SFR(X) derived from HMXB emission could be severely affected by stochastic effects since the flux would be dominated by a few binaries. The strong correlation found by Ranalli et al. extends to low values of the SFR ($\lesssim 0.1\,\mathrm{M_\odot\,yr^{-1}}$), and the presence of LMXB that are not associated with the present star formation activity seems to be a minor effect. However, for galaxies with SFR smaller than $1\,\mathrm{M_\odot\,yr^{-1}}$ and masses typical of a spiral galaxy, the X-ray luminosities and the derived SFR(X) could have an important contribution from LMXB affecting the observed correlation. We estimate in what follows the X-ray luminosity due to LMXB. Grimm, Gilfanov & Sunyaev (2002) found a relation between the stellar mass and the total X-ray luminosity produced by LMXBs in the Galaxy. They compared the integrated luminosity function of galactic LMXB detected by the All-Sky Monitor aboard the Rossi X-Ray Timing Explorer and assumed a stellar mass for the Galaxy of $5\times10^{10}\,\mathrm{M_\odot}$, in order to get the X-ray luminosity per unit stellar mass due to LMXB:

$$L_\mathrm{X}(\mathrm{LMXB})\,(\mathrm{erg\,s^{-1}}) = 5\times10^{28} M_\mathrm{s}, \quad (4)$$

where the stellar mass ($M_\mathrm{s}$) is given in solar masses.

By combining the derived stellar masses (Table 3) with equation (4) we computed the luminosity produced by the LMXB and the percentage of the derived SFR(X) not related to the recent star

**Table 3.** Best template fit, estimated stellar mass ($M_\star$) and derived UV flux at 2000 Å (rest frame and extinction corrected). F2000* is the corrected flux combining optical, UV and *Spitzer* fluxes. Column 7 gives the derived SFR(UV) (in parenthesis, using the F2000* values). Column 8 is the SFR(X) (in parenthesis the SFR given by the hard X-rays for galaxies probably harbouring an obscured AGN). Column 9 represents the percentage of the SFR(X) that could be contaminated by the luminosity of LMXB.

| Name | Template | $M_\star$ ($\times 10^{10}\,M_\odot$) | Extinction curve | $A_V$ (mag) | Log F2000 ($\mu$Jy) | Log F2000* ($\mu$Jy) | SFR(UV) ($M_\odot\,yr^{-1}$) | SFR(X) ($M_\odot\,yr^{-1}$) | LMXB (per cent) | Notes |
|---|---|---|---|---|---|---|---|---|---|---|
| CDFS 017 | Sb | 14 | LMC | 0.45 | 0.61 | – | 13 | 866(1888) | 0.18 | (a) |
| CDFS 065 | Sc | 5.6 | MW | 1.85 | 1.51 | 1.42 | 14 | 7.6 | 8.0 | |
| CDFS 073 | Sa | 39 | Calzetti | 0.90 | 0.71 | 0.90 | 5.1 | 21 | 20 | |
| CDFS 078 | Sc | 0.87 | LMC | 0.40 | 1.20 | 1.08 | 2.0 | 43(82) | 0.22 | (a) |
| CDFS 088 | Sc | 11 | LMC | 0.60 | 1.19 | 1.60 | 33 | 1212(8321) | 0.10 | (a) |
| CDFS 129 | Sc | 2.4 | MW | 1.50 | 1.43 | 1.83 | 5.9 | 8.9 | 3.0 | |
| CDFS 132 | Sc | 0.62 | LMC | 0.10 | 0.83 | 0.84 | 1.5 | 2.5 | 2.7 | |
| CDFS 149 | Sc | 0.26 | LMC | 0.40 | 0.95 | 1.02 | 0.57 | 2.5 | 1.1 | |
| CDFS 152 | M82 like | 0.92 | LMC | 0.25 | 1.27 | 1.12 | 4.9(3.4) | 2.9 | 3.4 | (b) |
| CDFS 158 | Sc | 1.5 | LMC | 0.45 | 0.80 | 1.10 | 4.0 | 11 | 1.4 | |
| CDFS 167 | Sb | 16 | Calzetti | 0.95 | 0.86 | 0.68 | 14 | 39 | 4.7 | |
| CDFS 185 | Arp 220 like | 0.13 | MW | 0.30 | 0.64 | 0.77 | 6.2 | 19 | 0.08 | |
| CDFS 189 | Sc | 2.1 | LMC | 0.65 | 2.36 | 2.47 | 4.4 | 2.6 | 9.0 | |
| CDFS 192 | Sc | 1.9 | LMC | 0.70 | 2.18 | 2.27 | 3.9 | 2.5 | 8.3 | |
| CDFS 196 | M82 like | 2.4 | LMC | 0.55 | 0.80 | 1.05 | 17.0 | 45 | 0.58 | |
| CDFS 207 | Arp 220 like | 1.2 | MW | 2.85 | 2.92 | 0.94 | 40(0.42) | 1.5 | 8.5 | (b) |
| CDFS 213 | Sc | 2.2 | MW | 1.50 | 2.62 | 2.26 | 4.7(2.1) | 0.22 | 110 | (c,d) |
| CDFS 228 | Arp 220 like | 0.54 | LMC | 2.35 | 2.47 | – | 19 | 1.7 | 3.6 | |
| CDFS 236 | M82 like | 1.5 | LMC | 0.20 | 0.94 | 1.54 | 9.4 | 18 | 0.91 | |
| CDFS 238 | Sc | 1.2 | MW | 1.20 | 1.07 | 1.21 | 2.9 | 2.7 | 4.7 | |
| CDFS 240 | Sc | 6.5 | LMC | 1.25 | 1.60 | 2.07 | 17 | 160(2783) | 0.45 | (a) |
| CDFS 265 | M82 like | 7.4 | Calzetti | 1.30 | 1.61 | 1.62 | 46 | 34 | 2.4 | |
| CDFS 267 | Arp 220 like | 0.02 | LMC | 0.55 | 1.45 | 1.40 | 0.67 | 0.44 | 0.51 | |
| CDFS 270 | Sc | 9.7 | LMC | 1.95 | 2.65 | 1.57 | 21(1.8) | 7.3 | 15 | (b) |
| CDFS 291 | Sc | 2.8 | LMC | 0.90 | 2.19 | 1.63 | 6.1(1.7) | 1.5 | 21 | (b) |
| CDFS 292 | Arp 220 like | 0.73 | Calzetti | 0.55 | 1.68 | 1.84 | 31 | 28 | 0.28 | |
| CDFS 294 | Sc | 1.5 | MW | 0.75 | 1.82 | – | 3.3 | 2.0 | 8.4 | |
| CDFS 304 | Sb | 8.0 | Calzetti | 0.95 | 0.83 | – | 6.1 | 189(1587) | 0.47 | (a) |
| CDFS 325 | Sc | 3.5 | MW | 0.75 | 1.21 | – | 9.2 | 164(577) | 0.23 | (a) |

Notes on individual galaxies: (a) possible obscured AGN; (b) galaxies in which we used the *Spitzer* data to correct the observed UV fluxes; (c) extremely weak in X-ray and (d) high contamination due to LMXB.

formation activity. The obtained values presented in Table 3 show that the contamination of the estimated SFR(X) due to LMXB is lower than 20 per cent for all the cases except for CDFS 213. In fact the X-ray luminosity of CDFS 213 could be fully explained as due to emission from LMXBs. This 'extreme' galaxy is further discussed in Section 5. In order to visualize the LMXB contribution to the SFR(X), we calculated the X-ray luminosity for a star-forming galaxy having a stellar mass somewhere between the prototype starburst galaxy (M82; stellar mass $M_s = 5 \times 10^9\,M_\odot$; Mayya et al. 2006) and the typical mass of a spiral galaxy like the MW ($M_s = 5 \times 10^{10}\,M_\odot$; Grimm et al. 2002). We took arbitrarily $M_s$ as five times larger than that of M82 and represented the corresponding SFR(X) in Fig. 2 by a dotted line.

Fig. 3 shows the histogram of the logarithm of the ratio between the SFR(X) and SFR(UV) ($\Delta$XUV). The histogram shows clearly that for the majority of the galaxies the SFR(X) is similar to SFR(UV), and that there are five galaxies with $\Delta$ XUV $> 1$, and one galaxy with $\Delta$ XUV $< -1$. The nature of these galaxies is discussed in the next section.

## 5 CONTAMINATION BY HIDDEN AGN AND THE DISCOVERY OF X-RAY WEAK GALAXIES

Figs 2 and 3 show that most of the galaxies (~62 per cent of the sample) lie within $\pm 0.5$ dex of the line which defines SFR(UV) = SFR(X) ($\Delta$XUV = 0) consistent with them being normal star-forming galaxies. However, when SFR(UV) is higher than $5\,M_\odot\,yr^{-1}$ the scatter is significantly larger. Similar amounts of scatter reaching lower SFRs are found in other samples of galaxies when Seyfert 2 and LINER galaxies are included in the relation between the SFR and the X-ray luminosity (e.g. Ranalli et al. 2003).

The large scatter seems to be related to two different phenomena: (i) galaxies that could be contaminated by the presence of very obscured AGN that will cause the X-rays to be bright and the UV to be faint, and (ii) X-ray weak galaxies due to a small number of HMXB for a given SFR, or to an overcorrection of the observed UV fluxes. All galaxies with SFR(X) higher than $100\,M_\odot\,yr^{-1}$ show a $\Delta$XUV larger than 1; they could be contaminated by a very obscured AGN not present in the optical SED but which nevertheless is powering the X-rays (Comastri et al. 2001; Maiolino et al. 2003, and references therein). Fig. 4 shows Very Large Telescope (VLT) spectra of three of these galaxies for which $\Delta$XUV is larger than 1. The spectra were extracted from Szokoly et al. (2004).[4]

CDFS 088 is the only one of the three galaxies that shows high excitation emission lines (e.g. [Ne v]) and strong oxygen lines

[4] Szokoly et al. spectra obtained from the dedicated page: http://www.mpe.mpg.de/CDFS/data

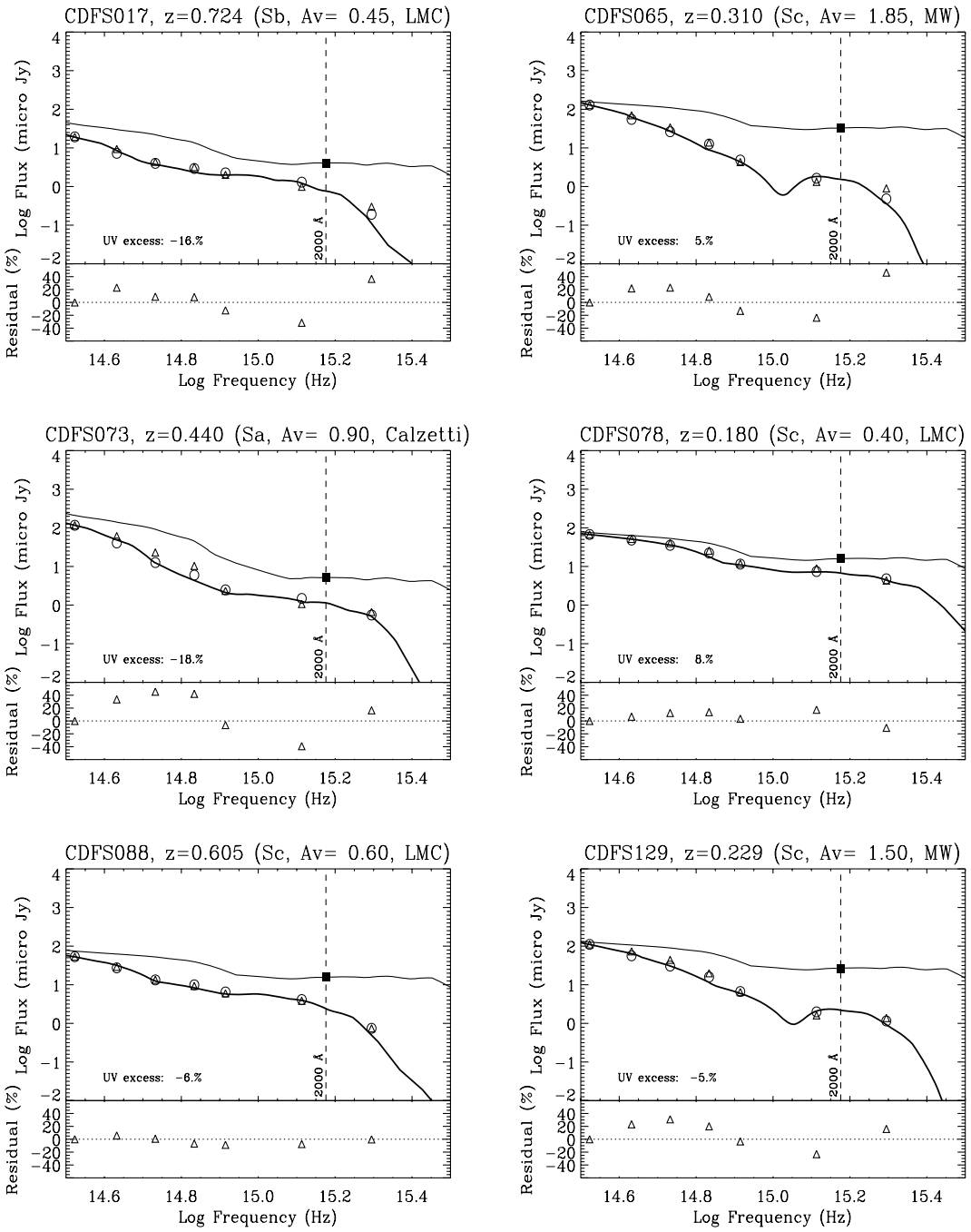


**Figure 1.** SEDs of the selected galaxies. Triangles are the observed values; circles are the fluxes extracted from the modelled spectra redshifted and without extinction correction (thick line). The thin line is the intrinsic template at rest frame without extinction. The black square is the rest-frame flux at 2000 Å. On top of each panel is the redshift, and the result of the best fit (i.e. galaxy template, visual extinction and extinction law). The UV excess (bottom left-hand corner of the panel) represents the difference between the observed NUV and FUV fluxes and the corresponding values given by the best-fitting model and is defined in Section 3.

suggestive of nuclear activity. The other two galaxies do not present strong emission lines. They are classified as normal galaxies (note that Szokoly et al. 2004 classified these two galaxies as low emission line galaxies). We would like to remark, however, that strong optical lines due to the presence of an AGN could have fallen outside the spectral optical range.

Hard X-rays may indicate that an AGN is present and this can be tested by calculating the SFR given by hard X-rays [$SFR^{hard}(X)$], and comparing it to the SFR(X) given by the soft band.

All the galaxies with SFR(X) higher than $100\,M_\odot\,yr^{-1}$ were detected in the hard X-ray band (Tables 1 and 3). The corresponding SFR was calculated as (Ranalli et al. 2003)

$$SFR^{hard}(X)\left(M_\odot\,yr^{-1}\right) = 2\times10^{-40}L_{2-10\,keV}\,(erg\,s^{-1}). \quad (5)$$

The calculated $SFR^{hard}(X)$ in these galaxies is higher than that obtained from the soft X-rays (see solid circles in Fig. 2), supporting the presence of an obscured AGN (or partially obscured as for CDFS 088).

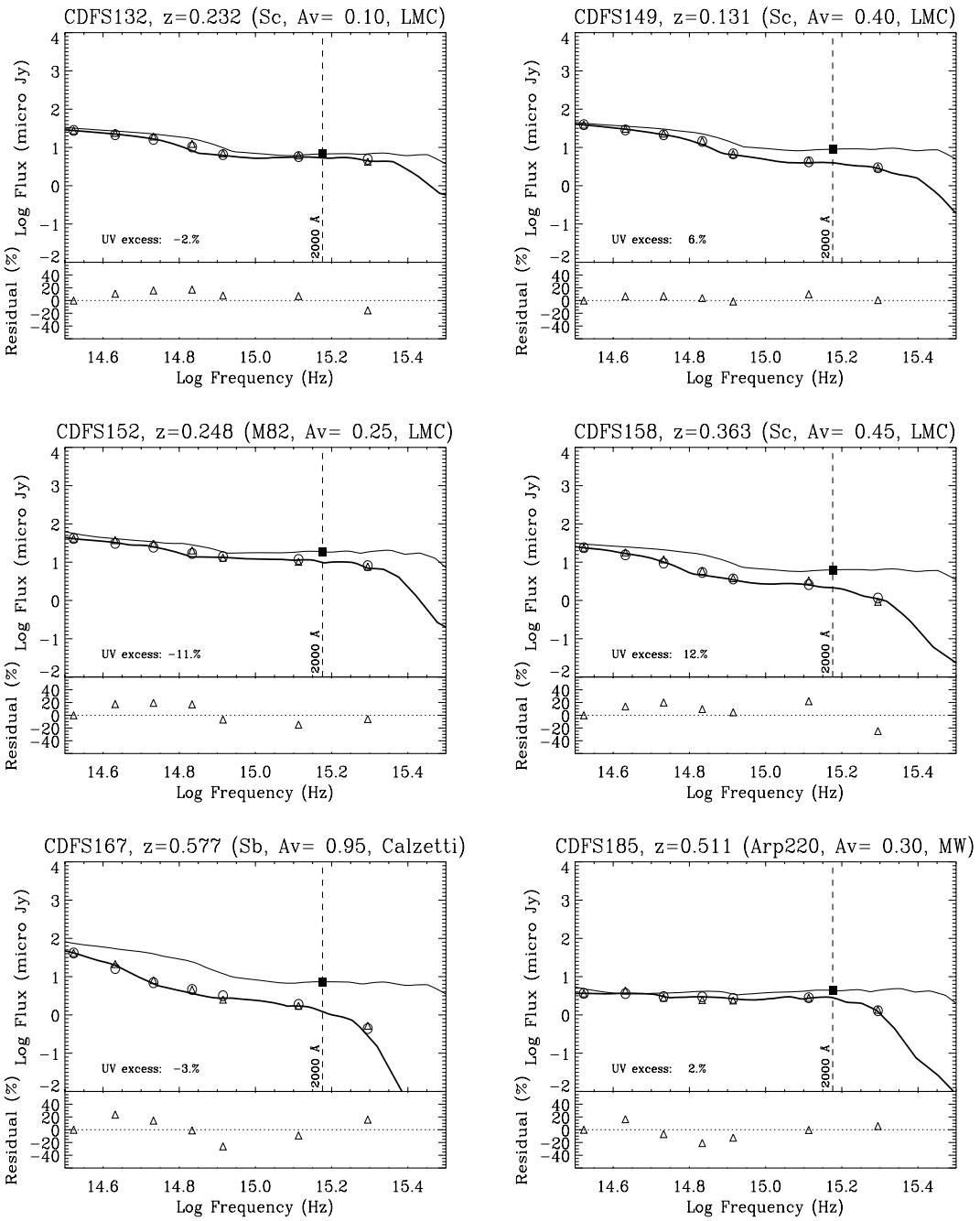


**Figure 1** – *continued*

The given SFR(X) in the soft and hard bands are based on the empirical results from Ranalli et al. (2003) which compared the X-ray with IR and radio luminosities closely related to recent star-forming events. The observed scatter is around 0.3 dex covering the X-ray luminosity range from $10^{38}$ to $10^{42}$ erg s$^{-1}$. If the observed luminosities are due to LMXB, an X-ray luminosity of $4.5 \times 10^{41}$ erg s$^{-1}$ (equivalent to a SFR of 100 $M_\odot$ yr$^{-1}$) would imply the existence of a galaxy with an unfeasible stellar mass of about $10^{13}$ $M_\odot$. In all the galaxies with SFR(X) greater than 100 $M_\odot$ yr$^{-1}$ and ΔXUV higher than 1 the estimated contamination due to LMXB is lower than 1 per cent (Table 3). The suggestion being therefore that most of the X-ray luminosity for these objects is related to the presence of a central massive black hole, and the contribution due to LMXB and star-forming processes is quite small.

CDFS 078 is one of the galaxies for which ΔXUV is higher than 1. In this case the SFR(UV) is about 2 $M_\odot$ yr$^{-1}$ but the SFR(X) is 43 and the SFR$^{\rm hard}$(X) is close to 100. Unfortunately this galaxy has no optical spectrum but it seems to be a low luminosity counterpart of the possible active galaxies discussed above.

Notice that for galaxies with Δ XUV > 1, the absolute value of the UV excess defined as the difference between the observed UV flux and the flux given by the model is below 20 per cent, therefore, the model seems to be a good representation of the stellar content of the galaxy and the observed UV fluxes are not heavily affected by the presence of an AGN.

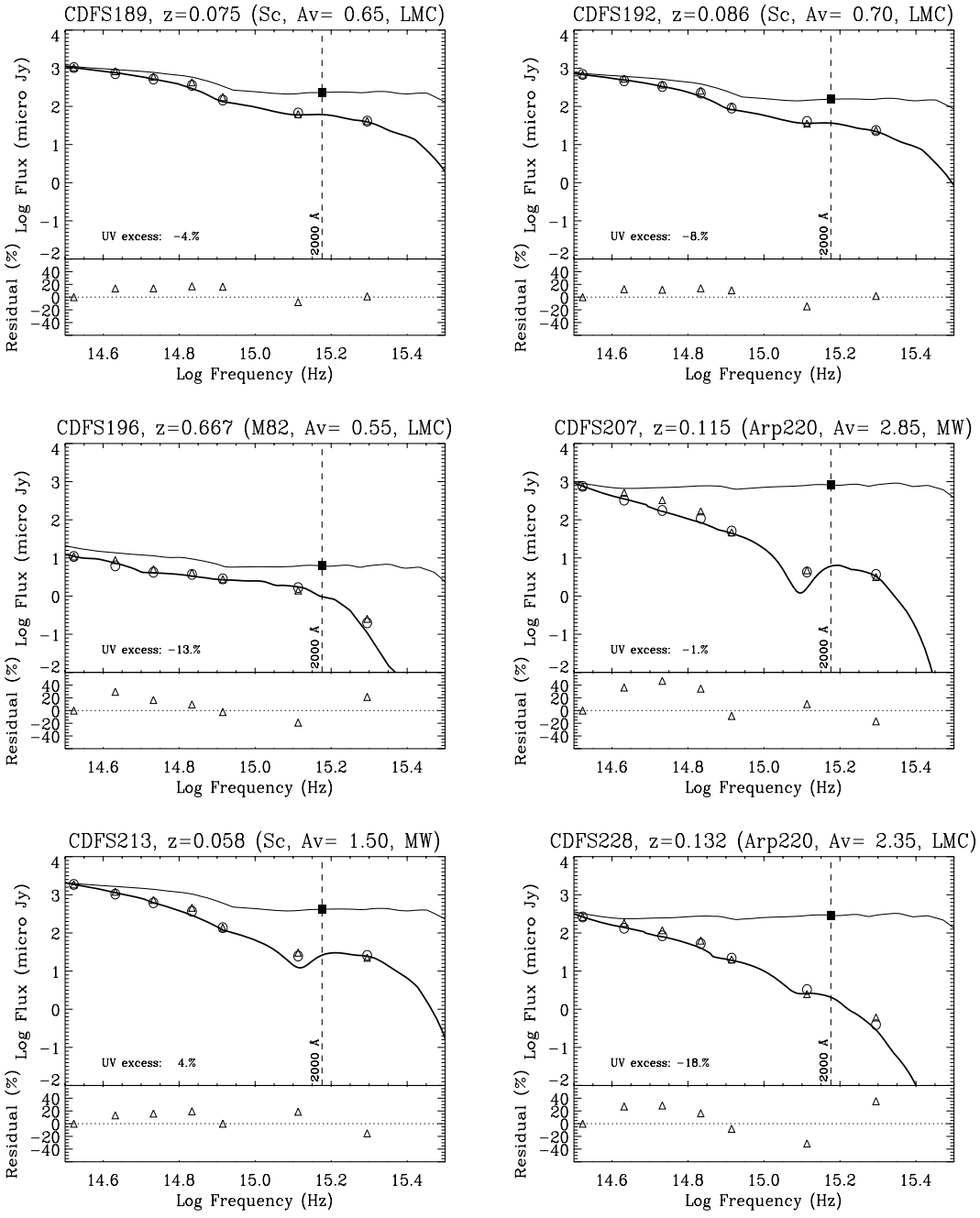


**Figure 1** – *continued*

In any case, we cannot rule out the presence of an obscured, compact and very powerful star-forming region of which we are only detecting a small fraction of the produced UV-optical emission. This effect known as *age selective extinction* is observed in the central regions of powerful starburst galaxies (e.g. Mayya et al. 2004).

(ii) Two galaxies CDFS 207 and CDFS 228 with SFR(UV) higher than 15 $M_\odot$ yr$^{-1}$ show very low X-ray emission implying SFR(X) of about 1.5 $M_\odot$ yr$^{-1}$. These galaxies are the most obscured ones in our sample ($A_V = 2.85$ and 2.35, respectively) and are compatible with an Arp 220-like template. Of them, only CDFS 228 was detected in the hard X-rays band, and the deduced $\mathrm{SFR}^{\mathrm{hard}}(\mathrm{X}) \sim 7$ is still six times lower than the corresponding SFR(UV).

For Arp 220, the ratio between the X-ray luminosities and the UV corrected by extinction $L_\mathrm{X}/(\nu\, L_\mathrm{UV}) = 1.7 \times 10^{-3}$ (UV data obtained from Goldader et al. 2002 and X-ray data from Iwasawa et al. 2001) is similar to the values obtained for CDFS 185 and CDFS 207 of $1.2 \times 10^{-3}$ and $1.6 \times 10^{-3}$, respectively. However, CDFS 228 has a value of $L_\mathrm{X}/(\nu\, L_\mathrm{UV}) = 4 \times 10^{-5}$ indicating that we are probably overestimating the UV corrections. Unfortunately this galaxy was not observed by *Spitzer* so we could not further analyse the correction factor applied to the UV fluxes as discussed in the following section. The ratio $L_\mathrm{X}/(\nu\, L_\mathrm{UV})$ for the other two galaxies fitted with an Arp 220-like spectrum is about a factor of 4 below the Arp 220 value.

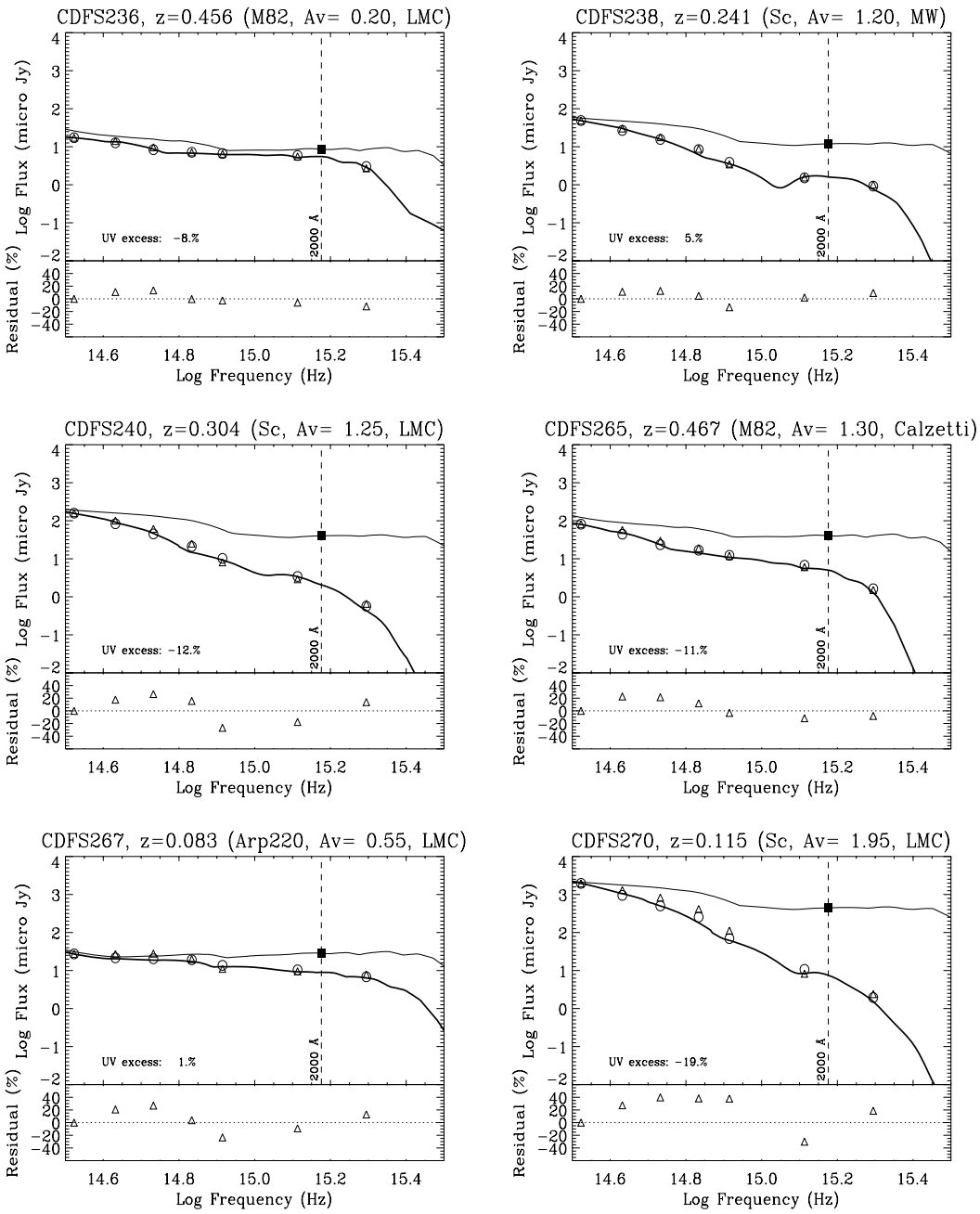


**Figure 1** – *continued*

Another extreme galaxy is CDFS 213 where an important fraction of the observed X-ray flux could be due to the presence of LMXBs (see Fig. 2). In any case, even if the observed X-ray flux has a strong contribution from LMXBs which are not related to a recent burst, the estimated ΔXUV is smaller than −1. For estimating the SFR(X) in this galaxy, we are using the flux provided by Giacconi et al. (2002) instead of the upper limit provided by Alexander et al. (2003). If we consider that the observed X-ray luminosity is just an upper limit, the nature of this galaxy would be even more extreme.

X-ray emission in the youngest objects is dominated by HMXB, therefore, a delay between the stellar UV continuum from massive stars [proportional to SFR(UV)] and the first compact object that is created after a supernova event [responsible for the deduced SFR(X)] is expected. A similar delay between the formation of stellar clusters and the production of compact objects after supernova explosions is observed in radio. In fact, the lack of synchrotron radiation has helped to identify young bursts of less than ∼20 Myr (Rosa-González et al. 2007).

There is always the possibility that we are just overestimating the correction factors applied to the UV fluxes and therefore we are not observing young objects. It has been indicated that in some cases the fluxes in the UV range could be badly estimated (e.g. Buat et al. 2005; Burgarella, Buat & Iglesias-Páramo 2005). We explore this possibility in the next section using *Spitzer* observations of the CDFS.

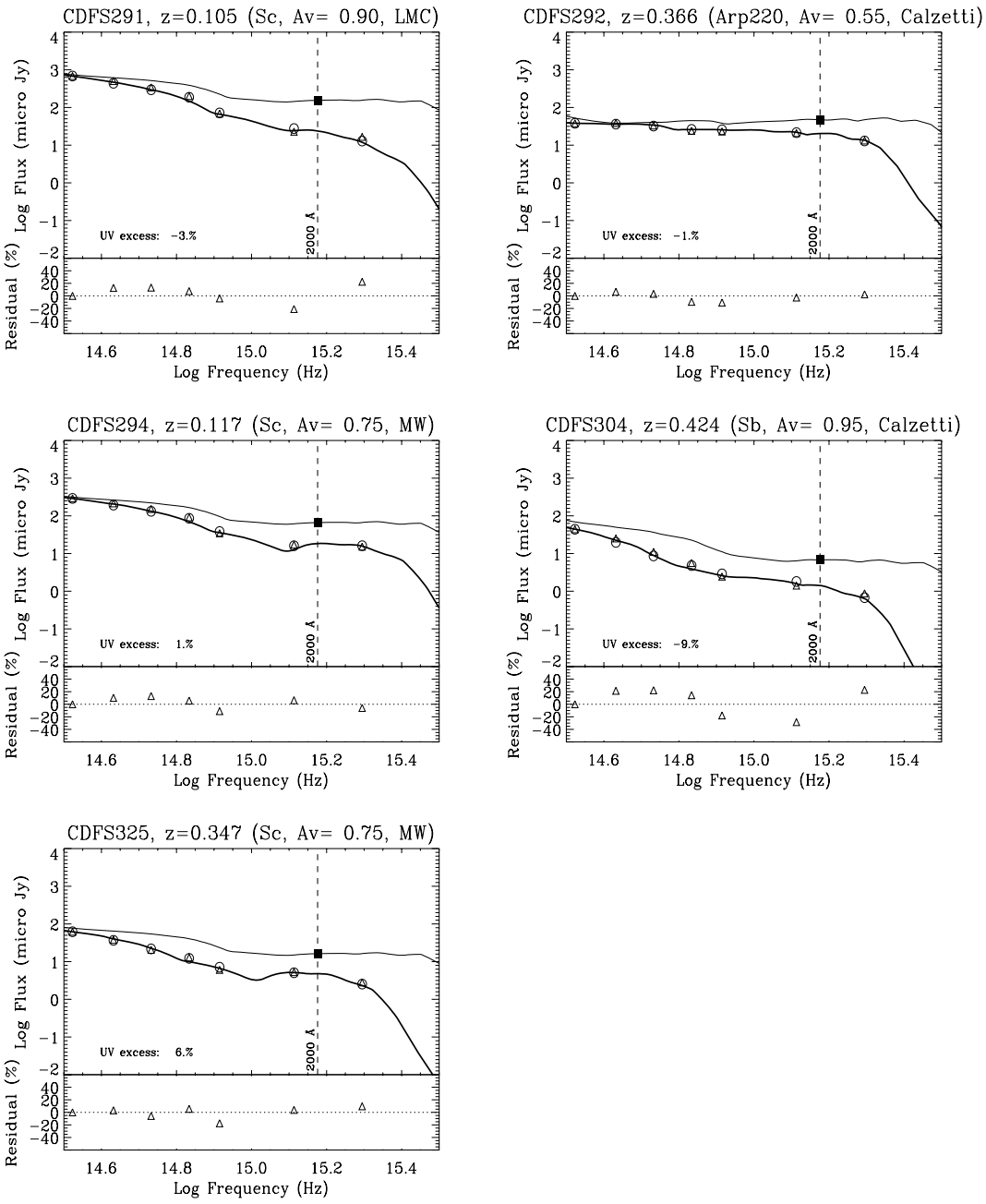


**Figure 1** – *continued*

## 6 ANALYSIS OF *SPITZER* DATA

The release (DR3) of the GOODS, one of *Spitzer's* Legacy Science Programs, includes Multiband Imaging Photometer for *Spitzer* (MIPS)[5] 24-μm images for GOODS-S and the corresponding source list.[6] Table 4 shows the fluxes at 24 μm ($S_{24}$) obtained by *Spitzer* for our sample of CDFS galaxies. Notice that five galaxies were outside the *Spitzer* coverage. The *Spitzer* fluxes are from DR3 except for galaxies with a *Spitzer* index of 000 (see Table 4). The fluxes of these galaxies were extracted directly from the scientific maps, using the conversion factor between observed counts and fluxes provided by the GOODS team (e.g. Dickinson & GOODS 2004).

To estimate the total IR luminosities (integrated between 8 and 1000 μm) the 24-μm luminosities obtained from the observed fluxes were transformed to IR luminosities using the empirical relation given by Takeuchi et al. (2005)

$$\log L_{\rm IR} = 2.01 + 0.878 \log L\,(25\,\mu{\rm m}), \quad (6)$$

where both luminosities are given in solar units. This relation is based on the study of 1420 galaxies with available data in the four *IRAS* bands. Takeuchi et al. (2005) show that this formulation provides good estimates of the total IR flux in a wide variety of galaxies including extreme galaxies such as Arp 220.

[5] The MIPS is fully described in Rieke et al. (2004).
[6] http://data.spitzer.caltech.edu/popular/goods/Documents/[4]goods_dataproducts.html

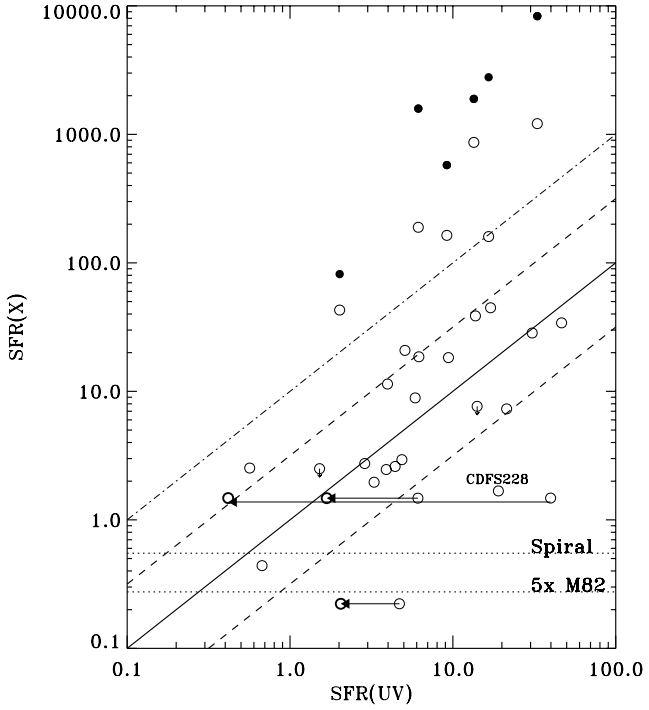


**Figure 2.** Open circles represent the SFR given by the UV versus the SFR given by the soft X-ray [$SFR^{soft}(X)$]. The solid line represents equal values and the dashed lines a deviation of 0.5 dex. Solid circles are the SFR calculated using the hard X-ray [$SFR^{hard}(X)$] for the galaxies with ΔXUV greater than 1 (dot–dashed line). The arrows point to the SFR(UV) calculated using the empirical relation between the FIR luminosity and the extinction in the UV for galaxies with $\Delta$ XUV $\leqslant -0.5$ detected by *Spitzer*. CDFS 228, the outlier not observed by *Spitzer*, is marked. The horizontal dotted lines show the contamination due to LMXB for a galaxy with five times more stars than M82 and for a typical spiral galaxy, as labelled (see text).

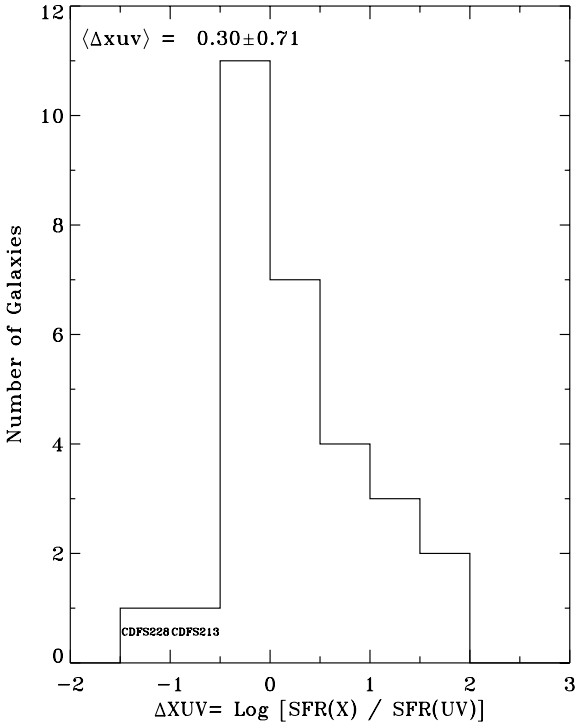


**Figure 3.** Histogram of the relation between the SFR given by the UV and by the X-rays. The mean and standard deviation are shown at the top.

The derivation of the $L(25\,\mu m)$ from the observed $S_{24}$ fluxes requires to assume a SED and to estimate the corresponding *K*-correction. For each galaxy we used the template obtained by the optical fit described in Section 3 but instead of using templates that only contain stellar light we use those with dust emission included. A full description of the templates and the application to model galaxies is given in several papers by the GRASIL group (e.g. Silva et al. 1998; Panuzzo et al. 2005; Vega et al. 2005). The luminosity at a given frequency ($\nu$) is given by

$$L_\nu = 4\pi D_L^2 \frac{S_{\nu o}}{(1+z)}, \tag{7}$$

where $D_L$ is the luminosity distance, $S_{\nu o}$ is the observed flux at 24 μm, $z$ is the redshift of the source and $\nu = \nu o\,(1+z)$. Once we get $L_\nu$ we normalize the corresponding template to this value and find the luminosity at $\lambda = 25\,\mu m$.

### 6.1 Using the FIR to correct dust attenuation

We have explored the possibility that galaxies with $\Delta$ XUV $\leqslant -0.5$ are outliers in Fig. 2 because the estimated dust attenuation is biased or not accurate enough in the absence of FIR constraints.

To this end we computed from the observed FIR a new value for the corrected flux at 2000 Å (F2000*), combining the IR luminosities obtained in the previous section with the *GALEX* data. Following Burgarella et al. (2005), the extinction in the *GALEX* bands ($A_{FUV}$ and $A_{NUV}$) is related to the IR flux ($F_{IR}$) by

$$\begin{aligned} A_{FUV} &= -0.028[\log(F_{IR}/F_{FUV})]^3 \\ &\quad + 0.392[\log(F_{IR}/F_{FUV})]^2 \\ &\quad + 1.094[\log(F_{IR}/F_{FUV})] + 0.546, \\ A_{NUV} &= -0.075[\log(F_{IR}/F_{NUV})]^3 \\ &\quad + 0.639[\log(F_{IR}/F_{NUV})]^2 \\ &\quad + 0.673[\log(F_{IR}/F_{NUV})] + 0.260, \end{aligned} \tag{8}$$

where $F_{FUV}$ and $F_{NUV}$ are the rest-frame FUV and NUV fluxes, respectively. $F_{FUV}$ and $F_{NUV}$, together with the rest-frame F2000, were measured from the fitted spectrum obtained in Section 3. Relation (8) was used to obtain the extinction in the FUV and NUV and the extinction at 2000 Å was calculated as the mean value of $A_{FUV}$ and $A_{NUV}$. The extinction corrected F2000 (F2000*) was used to estimate the corrected SFR(UV).

The results of this correction are shown in Fig. 2, where the arrows connect the original SFR(UV) with the new corrected values. In two cases (CDFS 207 and CDFS 291) the new values are much closer to the SFR(X), but for CDFS 213 the new SFR(UV) is still below the SFR given by the X-ray luminosities by a factor of about 10. This difference between the SFR estimators will remain even after taking into account that CDFS 213 may be affected by the presence of LMXBs as showed in Fig. 2 and discussed in Section 4.

Unfortunately CDFS 228 (labelled in the figure) is outside the *Spitzer* field of view and it was not possible to perform for it the analysis just discussed.

### 6.2 Infrared SFR

A significant fraction of the optical and UV light emitted by young and massive stars is absorbed by dust grains and re-emitted in the

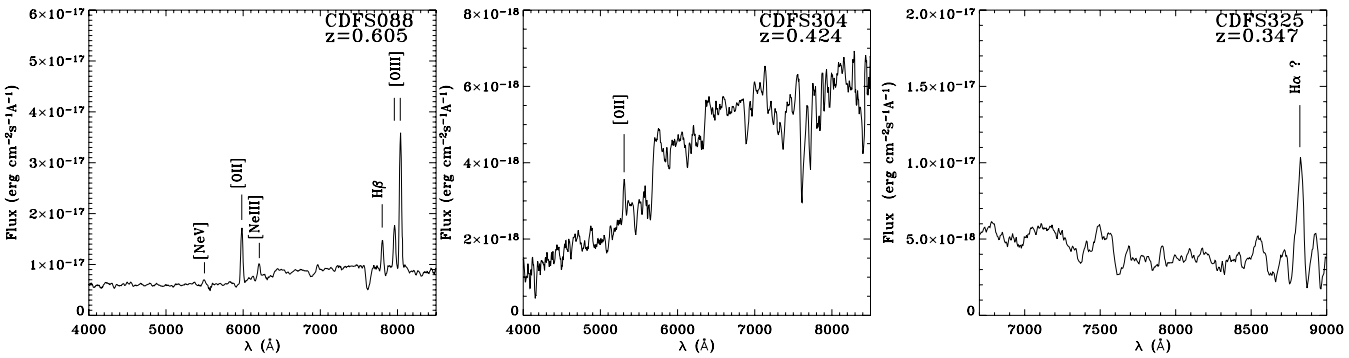


**Figure 4.** VLT spectra of three of the five galaxies with Δ XUV > 1. The spectra were extracted from Szokoly et al. (2004).

**Table 4.** IR data from *Spitzer*. The columns are galaxy name, *Spitzer* index from the DR3, flux and error at 24 μm, IR luminosity and estimated SFR.

| Name | *Spitzer* index | $S_{24}$ (μJy) | Error (μJy) | Log $L_{IR}$ (erg s$^{-1}$) | SFR(IR) (M$_\odot$ yr$^{-1}$) |
|---|---|---|---|---|---|
| CDFS 065 | 279 | 1.06E+03 | 8.28E+00 | 44.52 | 15 |
| CDFS 073 | 784 | 1.00E+02 | 3.28E+00 | 44.02 | 4.7 |
| CDFS 078 | 000 | 81.0E+00 | 12.0E+00 | 43.06 | 0.52 |
| CDFS 088 | 127 | 7.74E+02 | 9.36E+00 | 45.08 | 54 |
| CDFS 129 | 75 | 3.31E+03 | 2.13E+01 | 44.67 | 21 |
| CDFS 132 | 000 | 28.0E+00 | 5.60E+00 | 42.86 | 0.32 |
| CDFS 149 | 850 | 1.40E+02 | 4.21E+00 | 42.92 | 0.38 |
| CDFS 152 | 000 | 40.0E+00 | 04.8E+00 | 43.08 | 0.54 |
| CDFS 158 | 289 | 2.25E+02 | 4.71E+00 | 44.06 | 5.1 |
| CDFS 167 | 000 | 21.0E+00 | 4.20E+00 | 43.77 | 2.6 |
| CDFS 185 | 000 | 31.0E+00 | 4.30E+00 | 43.90 | 3.6 |
| CDFS 189 | 189 | 7.59E+03 | 7.59E+02 | 44.01 | 4.6 |
| CDFS 192 | 178 | 4.66E+03 | 4.66E+02 | 43.93 | 3.8 |
| CDFS 196 | 304 | 1.40E+02 | 5.65E+00 | 44.55 | 16 |
| CDFS 207 | 159 | 1.93E+02 | 4.32E+00 | 42.95 | 0.40 |
| CDFS 213 | 548 | 7.09E+03 | 7.09E+02 | 43.81 | 2.9 |
| CDFS 236 | 309 | 8.35E+02 | 6.62E+00 | 44.78 | 27 |
| CDFS 238 | 376 | 5.43E+02 | 4.62E+00 | 44.02 | 4.7 |
| CDFS 240 | 581 | 3.74E+03 | 4.34E+01 | 44.99 | 44 |
| CDFS 265 | 656 | 9.69E+02 | 6.88E+00 | 44.82 | 30 |
| CDFS 267 | 549 | 2.99E+02 | 3.81E+00 | 42.91 | 0.37 |
| CDFS 270 | 105 | 5.59E+02 | 4.97E+00 | 43.35 | 1.0 |
| CDFS 291 | 335 | 3.51E+02 | 5.95E+00 | 43.10 | 0.57 |
| CDFS 292 | 487 | 7.00E+02 | 9.35E+00 | 44.72 | 24 |

IR regime making this wavelength a good tracer of the current star formation activity as confirmed by multiple observations (e.g. Yun, Reddy & Condon 2001; Schmitt et al. 2006). A relation between the IR and the current SFR for normal galaxies is given by Kennicutt (1998)

$$\mathrm{SFR(IR)}\,(\mathrm{M}_\odot\,\mathrm{yr}^{-1}) = 4.5 \times 10^{-44} L_{\mathrm{IR}}\,(\mathrm{erg\,s}^{-1}). \quad (9)$$

Notice that $L_{IR}$ refers to the luminosity integrated over the full IR spectrum covering from 8 to 1000 μm, therefore, it is equivalent to the $L_{IR}$ calculated by equation (6).

The SFR(IR) computed using equation (9) is given in Table 4 and plotted against the SFR(UV) in Fig. 5. In general we find a good correlation between the SFR(UV) and the SFR(IR) for most of the sample galaxies detected by *Spitzer*.

CDFS 088 and CDFS 240, both with ΔXUV greater than 1, were detected by *Spitzer* and have a SFR(IR) similar to the SFR(UV), confirming that the observed X-ray luminosity is probably dominated by

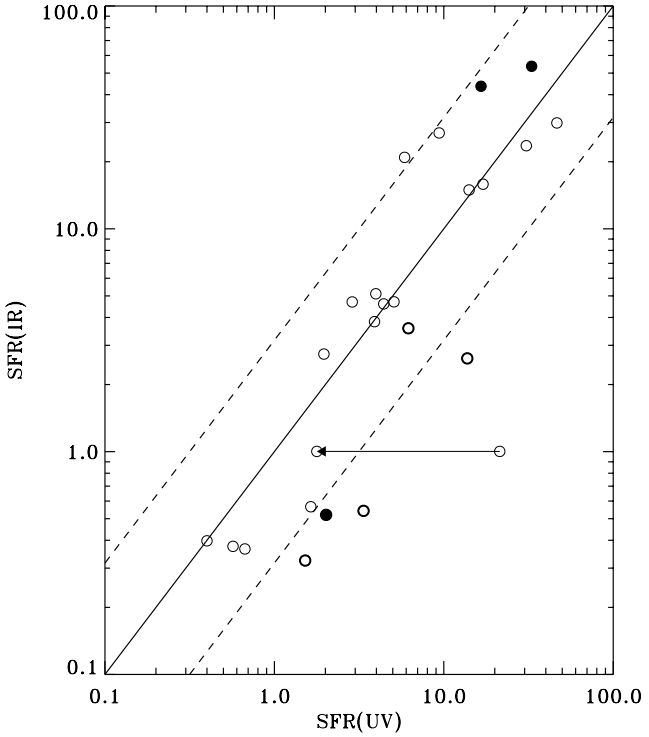


**Figure 5.** Comparison between the SFR(IR) and the SFR(UV) for the galaxies detected by *Spitzer*. Filled circles are the galaxies with ΔXUV greater than 1. Open circles are galaxies for which we extracted the 24-μm flux from the provided maps. The solid line represents equal values and the dashed lines a deviation of 0.5 dex. The arrow connects the SFR(UV) calculated using F2000 with the SFR(UV) using F2000* for CDFS 270.

nuclear activity while both UV and FIR are dominated by the stellar energy input. Unfortunately CDFS 017, CDFS 304 and CDFS 325 were outside the *Spitzer* fields and therefore not observed.

There is one galaxy, CDFS 270, that is quite far from the correlation showed in Fig. 5. The arrow plotted in Fig. 5 shows the result of applying the relation (8) to estimate the extinction in the UV range and to recalculate the luminosity and the corresponding SFR(UV) as explained in Section 6.1.

## 7 CONCLUSIONS

By comparing the SFR(UV) with the SFR(X) in star-forming galaxies selected from the CDFS, we have confirmed the use of the X-ray

luminosity as a reliable tracer of the current SFR even for galaxies with SFR as low as $1\,M_{\odot}\,yr^{-1}$.

The observed deviations can be explained by two different scenarios. In one case we are detecting obscured AGN in which the nuclear activity is not affecting the observed UV–optical SED. In this case the SFR(X) is at least one order of magnitude higher than the SFR(UV). For two of the sample galaxies (CDFS 088 and CDFS 240) where the ΔXUV is greater than 1, the SFR(IR) is similar to the SFR(UV) pointing to the fact that the nuclear activity is only affecting the output in the X-ray energy range.

We used empirical relations between UV and IR fluxes to set limits to the correction factors applied to the UV luminosities and the corresponding SFR(UV) and found that in most of the objects with negative values of ΔXUV the UV fluxes were overcorrected.

An extreme galaxy was found (CDFS 213) for which the X-ray luminosity is very low compared to the expected one based on SFR(UV). In this case we propose that the low X-ray luminosity is related to the delay between the peak of UV emission from massive stars – proportional to the SFR(UV) – and the later onset of the X-ray emission related to the formation of the first HMXBs. Thus our proposal implies that in CDFS 213 we are probably witnessing a very young burst that is intense in UV but has not yet fully developed its HMXB population. This suggests that the age of the burst is probably shorter than ∼20 Myr.

## ACKNOWLEDGMENTS

We thank Mónica Rodríguez, Divakara Mayya and Olga Vega for useful discussions. This research was partially supported by the French project PICS MEXIQUE # 2174 for collaborative research. Computer facilities for DR-G were kindly provided by *Dos-Informática*, Tenerife. DR-G, RT and ET acknowledge support by the Mexican Research Council (CONACYT) under grants 49942 and 40018. The *GALEX* data presented in this paper were obtained from the Multimission Archive at the Space Telescope Science Institute (MAST). STScI is operated by the Association of Universities for Research in Astronomy, Inc., under NASA contract NAS5-26555. Support for MAST for non-*Hubble Space Telescope* (*HST*) data is provided by the NASA Office of Space Science via grant NAG5-7584 and by other grants and contracts.

The authors are very grateful to an anonymous referee whose comments and suggestions largely improved the clarity of this paper.

## REFERENCES

Adami C. et al., 2005, A&A, 443, 805
Alexander D. M. et al., 2003, AJ, 126, 539
Babbedge T. S. R. et al., 2004, MNRAS, 353, 654
Bauer F. E., Alexander D. M., Brandt W. N., Hornschemeier A. E., Vignali C., Garmire G. P., Schneider D. P., 2002, AJ, 124, 2351
Bolzonella M., Miralles J.-M., Pelló R., 2000, A&A, 363, 476
Buat V. et al., 2005, ApJ, 619, L51
Burgarella D., Buat V., Iglesias-Páramo J., 2005, MNRAS, 360, 1413
Calzetti D., Kinney A. L., Storchi-Bergmann T., 1994, ApJ, 429, 582
Cerviño M., Mas-Hesse J. M., Kunth D., 2002, A&A, 392, 19
Comastri A. et al., 2001, in New Visions of the X-ray Universe in the XMM–Newton and Chandra Era. ESTEC, Noordwijk, Online-only reference (astro-ph/0203019)
Condon J. J., 1992, ARA&A, 30, 575
David L. P., Jones C., Forman W., 1992, ApJ, 388, 82
Dickinson M., GOODS, 2004, Bull. Am. Astron. Soc., 36, 1614
Fabbiano G., 1989, ARA&A, 27, 87
Ferreras I., Lisker T., Carollo C. M., Lilly S. J., Mobasher B., 2005, ApJ, 635, 243
Gabasch A. et al., 2004, ApJ, 616, L83
Giacconi R. et al., 2001, ApJ, 551, 624
Giacconi R. et al., 2002, ApJS, 139, 369
Giavalisco M. et al., 2004, ApJ, 600, L93
Goldader J. D., Meurer G., Heckman T. M., Seibert M., Sanders D. B., Calzetti D., Steidel C. C., 2002, ApJ, 568, 651
Grimm H.-J., Gilfanov M., Sunyaev R., 2002, A&A, 391, 923
Grimm H.-J., Gilfanov M., Sunyaev R., 2003, MNRAS, 339, 793
Howarth I. D., 1983, MNRAS, 203, 301
Iwasawa K., Matt G., Guainazzi M., Fabian A. C., 2001, MNRAS, 326, 894
Kennicutt R. C. J., 1998, ARA&A, 36, 189
Laird E. S., Nandra K., Adelberger K. L., Steidel C. C., Reddy N. A., 2005, MNRAS, 359, 47
Lilly S. J., Tresse L., Hammer F., Crampton D., Le Fevre O., 1995, ApJ, 455, 108
Madau P., Ferguson H. C., Dickinson M. E., Giavalisco M., Steidel C. C., Fruchter A., 1996, MNRAS, 283, 1388
Madau P., Pozzetti L., Dickinson M., 1998, ApJ, 498, 106
Maiolino R. et al., 2003, MNRAS, 344, L59
Mas-Hesse J. M., Kunth D., 1991, A&AS, 8, 399
Mayya Y. D., Bressan A., Rodríguez M., Valdes J. R., Chavez M., 2004, ApJ, 600, 188
Mayya Y. D., Bressan A., Carrasco L., Hernandez-Martinez L., 2006, ApJ, 649, 172
Morrissey P. et al., 2005, ApJ, 619, L7
Nandra K., Mushotzky R. F., Arnaud K., Steidel C. C., Adelberger K. L., Gardner J. P., Teplitz H. I., Windhorst R. A., 2002, ApJ, 576, 625
Osterbrock D. E., 1989, Astrophysics of Gaseous Nebulae and Active Galactic Nuclei. University Science Books, Mill Valley, CA
Panuzzo P., Silva L., Granato G. L., Bressan A., Vega O., 2005, in Popescu C. C., Tuffs R. J., eds, AIP Conf. Proc. Vol. 761, The Spectral Energy Distribution of Gas-Rich Galaxies: Confronting Models with Data, Am. Inst. Phys., New York, p. 187
Persic M., Rephaeli Y., Braito V., Cappi M., Della Ceca R., Franceschini A., Gruber D. E., 2004, A&A, 419, 849
Ranalli P., Comastri A., Setti G., 2003, A&A, 399, 39
Ravikumar C. D. et al., 2007, A&A, 465, 1099
Rieke G. H. et al., 2004, ApJS, 154, 25
Rosa-González D., Terlevich E., Terlevich R., 2002, MNRAS, 332, 283
Rosa-González D., Schmitt H. R., Terlevich E., Terlevich R., 2007, ApJ, 654, 226
Rosati P. et al., 2002, ApJ, 566, 667
Schmitt H. R., Calzetti D., Armus L., Giavalisco M., Heckman T. M., Kennicutt R. C., Leitherer C., Meurer G. R., 2006, ApJ, 643, 173
Seaton M. J., 1979, MNRAS, 187, 73
Silva L., Granato G. L., Bressan A., Danese L., 1998, ApJ, 509, 103
Szokoly G. P. et al., 2004, ApJS, 155, 271
Takeuchi T. T., Buat V., Iglesias-Páramo J., Boselli A., Burgarella D., 2005, A&A, 432, 423
Tozzi P. et al., 2001, ApJ, 562, 42
Van Bever J., Vanbeveren D., 2000, A&A, 358, 462
Vega O., Silva L., Panuzzo P., Bressan A., Granato G. L., Chavez M., 2005, MNRAS, 364, 1286
Wolf C. et al., 2004, A&A, 421, 913
Yun M. S., Reddy N. A., Condon J. J., 2001, ApJ, 554, 803

This paper has been typeset from a TEX/LATEX file prepared by the author.